

Aeroacoustic Source Strength Measurement of Helmholtz Resonator

Asami Nishikawa

May 19, 2011

University of Central Arkansas
Conway, AR 72035

The committee:

Advisor:

Dr. William V. Slaton, Ph. D.
Associate Professor of Physics and Astronomy

Reader:

Dr. Carl Frederickson, Ph. D.
Associate Professor of Physics and Astronomy

Department Chair:

Dr. Stephen Addison, Ph. D.
Professor and Chair, Department of Physics and Astronomy

Abstract

The characteristic of the aero-acoustic excitation of Helmholtz resonators with different neck geometries has been determined, and the work done to sustain and excite resonance has been studied. A Helmholtz resonator consists of a volume connected to a duct and has a well defined resonance frequency which depends on the length of the duct, the volume of the resonator and the cross-sectional area of the duct. In the system used during our measurements, two Helmholtz resonators have been positioned at opposite sides of a junction in a wind tunnel. The air flowing over the junction openings to the Helmholtz resonators can excite the acoustic resonance in the system. This is similar to blowing over an empty bottle's opening and creating a tone. The influence of the resonator's geometry has been observed in the measured acoustic amplitude and frequency in the resonator. The work done by the aero-acoustic source of sound has been determined through the measurement of the air speed in front of and behind the junction in the wind tunnel; and, the energy stored in the resonator has been determined through the measurement of the acoustic pressure inside the resonator.

Contents

1	Theory	5
1.1	Helmholtz Resonator	5
1.1.1	Introduction	5
1.1.2	Resonance	6
1.2	Strouhal Number	9
1.3	Energy Dissipation and Quality Factor	10
2	Experimental Setup	13
2.1	Whole System	13
2.2	Setup Surrounding the Flask	13
2.2.1	Calibration of the Pressure Sensor	14
2.3	Setup Surrounding Wind Tunnel	15
2.3.1	Wind Tunnel	15
2.3.2	Pitot-tube	16
2.4	Replaceable Necks	18
3	Results and Analysis	19
3.1	Frequency Measurement	19
3.2	Dimensionless Analysis: The Ratio $\frac{V_{ac}}{V_1}$ V.S. Strouhal number	19
3.3	Velocities Before and After the Opening of the Resonators	21
3.4	Aeroacoustic Source Strength	21
3.4.1	Energy Dissipation	22
3.4.2	Quality Factor	22
3.4.3	Energy Balance	23
4	Conclusion	24
5	Acknowledgements	25

6	Reference	26
7	Appendix	27
A	The Derivation of the Ratio, $\frac{\langle V \rangle}{V_{max}}$, for Turbulent Flow	27
B	The Measured Length of the Replaceable Duct Pieces.	28
C	Figures	29

1 Theory

When a person blows over the opening of an empty bottle with appropriate strength, a tone is produced. How does the air move inside the bottle and create the tone? How much energy is extracted from the moving air stream to excite and sustain the resonance? This thesis seeks to explore this phenomena in a wind tunnel with Helmholtz resonators.

An understanding of what a Helmholtz resonator is will be helpful to imagine the setup we have used. Also, it can be helpful to know how the movement of the air inside a Helmholtz resonator can be described as a mass-spring system. The air flow blowing over the opening of the resonator can create an acoustic resonance in the system. By measuring velocities before and after the opening, we can compute the work done to create the resonance. Additionally, the quantities describing the aeroacoustic source strength will be introduced.

1.1 Helmholtz Resonator

1.1.1 Introduction

By blowing over the opening of an empty bottle, a mass of air moves into the cavity through the neck. Then, the compression of the air in the cavity pushes the mass back to the opening. The system behaves similarly to a simple oscillator. We can model the air in the neck as a mass and the air in the cavity as a spring (See Fig.(1)) ¹. A Helmholtz resonator is an example of a lumped acoustic system illustrated in Fig.(2). This instrument is composed of a cavity of volume, V_0 , connected to a duct with the cross-sectional area, S_{neck} , and the neck length, L .

¹This is only valid for frequencies near the fundamental resonance frequency.

1.1.2 Resonance

Assuming the Helmholtz resonator is a mass-spring system, the fundamental resonance frequency is given by

$$f = \frac{1}{2\pi} \sqrt{\frac{k}{m}} \quad (1)$$

where m is the mass of air in the neck of the resonator, and k is the effective spring constant. First, consider the effective spring constant. Considering the thermodynamic equation for the speed of sound,

$$c^2 = \frac{B}{\rho_0} \quad (2)$$

where ρ_0 is the average air density, and B is the bulk modulus defined as

$$B = -V_0 \frac{\Delta P}{\Delta V} \quad (3)$$

where V_0 is the volume of the cavity, ΔP is the change in pressure inside the cavity, and ΔV is the change in volume caused by the air in the neck pushing into the cavity. Solving these equations for the pressure, ΔP ,

$$\begin{aligned} \Delta P &= -B \frac{\Delta V}{V_0} \\ &= -\rho_0 c^2 \frac{\Delta V}{V_0} \\ &= -\rho_0 c^2 \frac{(-\Delta x_{mass} S_{neck})}{V_0} \\ &= \frac{\rho_0 c^2 S_{neck}}{V_0} \Delta x_{mass} \end{aligned} \quad (4)$$

where Δx_{mass} is the displacement that the mass of air in the neck moves into the cavity. The force exerted on the mass due to the compressed air in the cavity is,

$$\begin{aligned} F &= -\Delta P S_{neck} \\ &= - \left\{ \frac{\rho_0 c^2 S_{neck}^2}{V_0} \right\} \Delta x_{mass}. \end{aligned} \quad (5)$$

Since the inside of the brace in Eq. (5) is constant, this looks like Hooke's law:

$$F = -k \Delta x_{mass} \quad (6)$$

where the effective spring constant of the air in the cavity is,

$$k = \frac{\rho_0 c^2 S_{neck}^2}{V_0}. \quad (7)$$

Considering an end correction [1], which accounts for the fact that part of the acoustic wave extends beyond the end of the pipe, the mass of the air in the neck is

$$m = \rho_0 S L' \quad (8)$$

where L' is the effective length for the Helmholtz resonator with flanged opening [1]

$$L' = 2(L + 1.7R_{neck}) \quad (9)$$

where the neck length is L , and the radius of the neck's cross section, R_{neck} . Therefore, the resonance frequency is,

$$f = \frac{c}{2\pi} \sqrt{\frac{2S_{neck}}{V_0 L'}}. \quad (10)$$

So, the frequency is dependent on S_{neck} , V_0 and L' . During this experiment, instead of S_{neck} and V_0 , we have chosen to vary L' to change the frequency. In our setup, it is the easiest to

change the neck length by using pieces of ducts with different lengths and coupling clamps. The position of the mass of air in the neck, x_{mass} , is assumed to move sinusoidally as

$$x(t) = A \sin(\omega t) \quad (11)$$

with a constant amplitude, A , and the angular frequency $\omega = 2\pi f$ where f is given by Eq.(10). Thus, the velocity of the mass is,

$$\frac{dx_{mass}}{dt} = A\omega \cos(\omega t) \quad (12)$$

$$= A \left(2\pi \frac{1}{T} \right) \cos(\omega t) \quad (13)$$

$$= V_{ac} \cos(\omega t) \quad (14)$$

where T is the period, and V_{ac} is the acoustic velocity amplitude of the air in the neck of the resonators, $\frac{2\pi A}{T}$. The change in the pressure inside the resonator is,

$$\Delta P = P_{amp} \sin(\omega t) \quad (15)$$

where P_{amp} is the pressure amplitude. However, using Eq. (5) the change in the pressure can be also expressed as

$$\begin{aligned} \Delta P &= \frac{\rho_0 c^2 S_{neck}}{V_0} \{ A \sin(\omega t) \} \\ &= \frac{\rho_0 c^2 S_{neck}}{V_0} \left\{ \frac{\omega A}{\omega} \right\} \sin(\omega t) \\ &= \frac{\rho_0 c^2 S_{neck}}{V_0} \left\{ \frac{2\pi A}{T} \right\} \sin(\omega t) \\ &= \frac{\rho_0 c^2 S_{neck}}{V_0} \left\{ \frac{V_{ac}}{\omega} \right\} \sin(\omega t) \\ &= \frac{\rho_0 c^2 S_{neck} V_{ac}}{V_0 \omega} \sin(\omega t) \end{aligned} \quad (16)$$

Comparing Eq. (15) and (16), the acoustic velocity amplitude in the neck is,

$$V_{ac} = \frac{V_0 \omega}{\rho_0 c^2 S_{neck}} P_{amp} \quad (17)$$

V_{ac} is proportional to P_{amp} .

1.2 Strouhal Number

The Strouhal number, St , characterizes the aero-acoustic excitation of the resonator with different neck geometries:

$$St = \frac{f D_{neck}}{V_1} \quad (18)$$

where D_{neck} is the diameter of the neck's cross-sectional circular area, f is the frequency, and V_1 is the velocity of the flow blowing over the opening of the Helmholtz resonator. Eq. (18) can be rewritten as,

$$St = \frac{f}{\frac{V_1}{D_{neck}}} = \frac{\frac{1}{T_{ac}}}{\frac{1}{\Delta t_1}} = \frac{\Delta t_1}{T_{ac}} \quad (19)$$

where T_{ac} is a period of the acoustic velocity, and Δt_1 is the time required for a particle of air to move by D_{neck} with the main flow V_1 . If St is small, it indicates that the gas takes a short time to cross the opening of the resonator (ie. fast flow). If St is large, it indicates that the gas takes a long time to cross the opening of the resonator (ie. slow flow). The St 's range for our experiment is shown in Fig.(20), ($0.1 \leq St \leq 0.25$). Considering Eq.(16), we can imagine the change of the pressure in the flask versus time in a period, 2π , like Fig.(3). The range of $0.1 \leq St \leq 0.25$ falls within the first quarter of a period.

In this one period, how does the air in the neck and cavity move? Fig. (3) shows the pressure in one flask, and Fig. (4) illustrates the movement of the air in the neck. During the first quarter of a period, the air in the neck is pushed into the cavity by the vortex which increases the pressure in the flask. Then, during the second and third quarter, the mass of air in the neck is pushed back by the air in the cavity into the cavity of the flask at the another side.

Finally, during the last quarter, the air is returned to its original position, and the pressure in the flask returns to its starting value. This movement of the air in the neck is like a child riding on a swing. At both openings of the resonators, a vortex is created when the mean flow passes over. This vortex is coiling up and pushing on the air in the neck and sustains the movement of air. This vortex is like the child's grandmother pushing and driving the swing. Note that the swing has a large amplitude when she pushes the child with good timing. The St indicates this good timing when the mean flow drives the air in the neck during the first quarter cycle of the pressure fluctuation in the flask.

1.3 Energy Dissipation and Quality Factor

By placing two Helmholtz resonators at opposite sides of a cross-junction in a wind tunnel, the air flowing over the junction openings to the Helmholtz resonators can excite the acoustic resonance of the system. Measuring the air flow velocities before and after the junction, V_1 and V_2 , the kinetic energy difference can be determined. This energy difference is the work done to excite and sustain the resonance and represents the total dissipated energy, $E_{dissipated}$, for the main flow. Some of $E_{dissipated}$ goes to energy stored in acoustics. In order to characterize the resonance of acoustic systems such as Helmholtz resonators, the quality factor is used,

$$Q = 2\pi \frac{E_{acoustic}}{E_{dissipated}}. \quad (20)$$

Looking into Q , first, let's think about $E_{acoustic}$. The mass of the air, m , in between the cavities of two Helmholtz resonators connected with a cross junction moves back and forth with V_{ac} . The mechanical energy of the mass of air can be expressed as

$$E_{acoustic} = \frac{1}{2}mV_{ac}^2 \quad (21)$$

Considering the volume of the mass of air in the neck, we can rewrite this as

$$E_{acoustic} = \frac{1}{2}(\rho_0 L_{total} S_{neck}) V_{ac}^2 \quad (22)$$

where L_{total} is the total effective neck length, twice the effective neck length of a single Helmholtz resonator.

Because of the energy dissipation, the velocity of the air flowing in the wind tunnel changes from V_1 (faster) to V_2 (slower) after the junction. By the work-kinetic energy theorem, $\Delta KE = W$ where ΔKE is the kinetic energy difference, and W is the work. Similarly to $E_{acoustic}$, using the mechanical energy expression,

$$E_{dissipated} = \frac{1}{2} m_d (V_1^2 - V_2^2) \quad (23)$$

where m_d is the mass of air flowing over the openings of Helmholtz resonators in a period of the resonance.

Assuming that a lump of air at the center of the circular cross sectional area flows linearly with constant acceleration, the basic kinematics is,

$$V_2^2 - V_1^2 = 2\alpha D_{12} \quad (24)$$

where α is the acceleration of the air flow, and D_{12} is the distance between the points where the velocities before and after the junction are measured. In a period of resonance, $t_{ac} = \frac{1}{f}$, the lump of air moves a distance,

$$L_d = V_1 t_{ac} + \frac{1}{2} \alpha t_{ac}^2, \quad (25)$$

and so Eq.(23) can be rewritten as

$$E_{dissipated} = \left| \frac{1}{2}(\rho_0 L_d S_{neck})(V_2^2 - V_1^2) \right|. \quad (26)$$

It can be expected that a bigger change in velocity results in a large dissipation of energy from the main flow.

Solving Eq.(24) for α and applying that to Eq.(25) yields,

$$L_d = V_1 t_{ac} + \frac{V_2^2 - V_1^2}{4D_{12}} t_{ac}^2. \quad (27)$$

Using Eq. (22) and (26), the quality factor (20) can also be written as,

$$Q = 2\pi \frac{L_{total}}{L_d} \frac{V_{ac}^2}{|V_2^2 - V_1^2|}. \quad (28)$$

From Eq. (28), we can say that the quality factor is the ratio of the energy stored in acoustics to the total dissipated energy. The quality factor indicates the efficiency of the conversion of flow energy into stored acoustic energy.

2 Experimental Setup

The measurements of velocities over the resonators' openings, the pressure inside the cavity, and the temperature inside the system have allowed us to determine the characteristic of the aero-acoustic excitation of the resonators and the work done to sustain and excite resonance. We will introduce the whole system for carrying out the measurements and look into the individual components: pressure sensor, pitot-tube, wind tunnel and replaceable necks.

2.1 Whole System

The system is composed of 2 inch ID glass pipe, a cross junction, various lengths of duct pieces and two glass 5L flasks (See Fig.(5)). In order to measure the quantities required to see the air flow's behavior, the following are used: an Omega HH501DK type K thermometer, a Hewlett 54663B Packard oscilloscope, a 175 Fluke true rms multimeter, two pitot-tubes, and two pressure sensors built from an Integrated Silicon Pressure Sensor MPX 5010 DP pressure sensor. One side of the wind tunnel is connected to a model QPL 650 shop vacuum which creates the flow and a TENMA variable auto transformer that adjusts the flow through changing the voltage supply to the vacuum. The transformer outputs 0-130(Vac) to operate the vacuum by adjusting the dial which is graduated to 130.

2.2 Setup Surrounding the Flask

One of the pressure sensors is used as a microphone to measure the amplitude of the acoustic pressure change, P_{amp} , and the frequency of oscillation in the flasks. The microphone signal is viewed on the oscilloscope. As the mean flow passes over the junction opening, a vortex is created. The creation of the vortex and its behavior influences the acoustic excitation of the flasks. Consequently, the acoustic behavior of the flasks influences the creation of the next vortex. In this way, a feedback loop is generated, which is shown to depend only on the geometry of the system and V_1 .

Another pressure sensor is used to measure the mean flow velocities of the air before and after the junction in the duct, V_1 and V_2 , via two pitot-tubes and valves connected to the two pitot-tubes and the sensor; and, it also can measure the pressure difference between the room and the inside of the duct for another pressure measurement.

Fig.(5) illustrates the whole system used during this experiment, and Fig. (6) illustrates the system around the pitot-tubes measuring the velocities in the main wind tunnel. In Figs. (5) and (6), the pressure sensors are illustrated as black boxes connected to the pitot-tubes and the microphone. The circuit diagram of the black boxes including an Integrated Silicon Pressure Sensor MPX 5010 DP is shown in Fig. (7)². The circle labelled “IPS” shows the Integrated Silicon Pressure Sensor itself, and the capacitors and a resistor work as a filter for the output signal. The LED is to show if the switch is on or off. The “IPS” itself operates with input voltage of 4.75-5.25(Vdc) and responds to the pressure 0-10(kPa).

2.2.1 Calibration of the Pressure Sensor

The pressure sensor connected to the pitot-tubes has been calibrated as a system with each pitot-tube (See Pitot-tube section). The other pressure sensor, the microphone inside the flask, has been calibrated with a water manometer and a syringe as illustrated in Fig. (8). The manometer measures a pressure difference by balancing the weight of a water column between two pressures created by the air and syringe. Changing the pressure inside the manometer by using a syringe, we could measure the pressure by the change of the water column’s height. Since body temperature does affect on the pressure measurement, it is important to do this calibration with care and few touches on the syringe, the manometer and so on. Fig. (9) is a plot of the pressure inside the manometer versus voltage read from the voltmeter connected to the pressure sensor. The calibration in Fig. (9) allows us to convert from the measurable voltage to the pressure. Also, it lets us compute the pressure

²It is left to the reader to calculate the value of the resistance to properly illuminate the LED.

amplitude using easily measurable variables,

$$P_{amp} = \left\{ \frac{1.003}{2} (V_{pp} - V_{pp0}) \right\} \times 10^3 (Pa), \quad (29)$$

in terms of V_{pp} is the peak-to-peak voltage (V) shown in the oscilloscope screen, and V_{pp0} is the quantity of V_{pp} when V_1 is 0 (m/s). V_{pp0} is changing for each set of measurements possibly due to ambient pressure and temperature changes. To account for this, we measure the value before each data run. The IPS pressure sensor has a response time of 1 ms. The highest resonance frequency in our measurement was 75.76 (Hz). Applying this quantity to the relationship, $T = \frac{1}{f}$, we have got the shortest period, 13.4 ms, in our measurement. Since the response time is shorter than the period of the fastest signal in our experiments, we can say that the pressure sensor responds quickly enough for this measurement.

2.3 Setup Surrounding Wind Tunnel

2.3.1 Wind Tunnel

In order to get uniform flow at the points where the pitot-tubes are located, it is nice to consider the entrance length of the wind tunnel's main duct. A dimensionless parameter known as the Reynolds number determines the nature of the flow, laminar or turbulent. The Reynolds number is generally said to be the ratio of inertial forces to viscous forces. The Reynolds number for a pipe or duct is defined as

$$Re = \frac{V_{ent} \rho D_{duct}}{\mu} \quad (30)$$

where V_{ent} is the flow velocity, ρ is the density of the fluid, D_{duct} is the diameter of the pipe or duct, and μ is the dynamic viscosity. The flow is defined as laminar if $Re < 2300$, transient if $2300 < Re < 4000$, and turbulent if $Re > 4000$.

As the result of measuring the area averaged V_{ent} at the upstream end of the wind tunnel

using a HHF92A Digital Anemometer, the range of the Reynolds number is from 36,500 to 105,000 for our experiment; therefore, the nature of the air flow into the wind tunnel can be assumed as turbulent. The length required to get fully developed uniform flow entering a tube is called the entrance length. The entrance length for turbulent flow is [3],

$$L_e \approx 4.4D_{duct}Re^{\frac{1}{6}}. \quad (31)$$

For our largest Reynolds number(105,000) and the wind tunnel diameter, we calculate a maximum entrance length of 1.54(m). So, we have designed the setup with the duct on the upstream side of the cross junction to be 1.81(m), which is longer than 1.54(m).

2.3.2 Pitot-tube

To measure the velocities inside the wind tunnel, two pitot-tubes placed before and after the junction have been connected to a pressure sensor by tubing like the one illustrated in Fig. (6). Using the bent tubing, we can measure the stagnation pressure. The bent tubing is visually aligned with the center of the duct. However, the placement is NOT critical if the velocity distribution is turbulent because the velocity around the center is about same as illustrated in Fig. (30). From the hole on the duct's wall at the same spot where the bent tubing's opening is at, we can read the static pressure. By the difference between these two kinds of pressures, we can know the flow velocity inside the duct from Bernoulli's equation. However, we calibrated the pitot-tubes with a HHF92A Digital Anemometer because of the individuality of each pitot-tube. Fig. (10) illustrates a model of the pitot-tube used in this measurement (See Fig. (11) for a photo of the switches illustrated in Fig. (6)). Each pitot-tube is calibrated to convert from voltage given by the pressure sensor to flow velocity directly. Positioning both the HHF92A Digital Anemometer and the pitot-tubes connected to the pressure sensor and a voltmeter in the main wind tunnel, we have compared the velocity read by the anemometer corresponding to each voltage read by the voltmeter (See

Fig. (12)). Fig. (12) is different from Fig. (5) and (6) because the calibration has been carried out using a straight section of wind tunnel instead of with the cross junction connected to flasks. The straight section is the same length as the cross-junction. The anemometer is designed to measure the cross-sectional surface area average velocity of the flow going through the propeller, however the pitot-tube is designed to measure the maximum velocity at the center of the duct. Assuming that the flow inside our system is turbulent, [2]

$$\frac{\langle V \rangle}{V_{max}} = 0.8 \quad (32)$$

where $\langle V \rangle$ is the surface average velocity, and V_{max} is the maximum velocity at the center of the duct (see Appendix A for this derivation). In our set up, this can be rewritten as

$$\frac{\langle V_{meter} \rangle}{V_{1\ or\ 2}} = 0.8 \quad (33)$$

where $V_{1\ or\ 2}$ is the velocity assumed to be measured by pitot-tube1 or pitot-tube2, and $\langle V_{meter} \rangle$ is the surface average velocity measured by the HHF92A Digital Anemometer at the end of the wind tunnel.

Since the cross-sectional surface areas of the duct and the anemometer are different,

$$\langle V_{1\ or\ 2} \rangle = \frac{S_{meter}}{S_{1\ or\ 2}} \langle V_{meter} \rangle \quad (34)$$

where $\langle V_{1\ or\ 2} \rangle$ is the surface average of $V_{1\ or\ 2}$, and S_{meter} and $S_{1\ or\ 2}$ are each cross sectional surface area of the anemometer and the duct where the pitot-tubes are positioned. Using the above two equations,

$$V_{1\ or\ 2} = \frac{1}{0.8} \frac{S_{meter}}{S_{1\ or\ 2}} \langle V_{meter} \rangle \quad (35)$$

The relationships between the velocities measured at the center of the duct and the voltage shown on the voltmeter connected to the pitot-tubes and pressure sensor are plotted in Fig. (13) and (14). From the plots, we can compute the conversion equation from voltage to

velocity ³

$$V_1 = \frac{-0.0003757 + \sqrt{(0.0003757)^2 + 4(0.0005476)(Vol_{1i} - Vol_1)}}{2(-0.0005476)} \quad (36)$$

where $Vol_{1i}(V)$ is the initial voltage measured at the pitot-tube1 when $V_1 = 0(\text{m/s})$, and $Vol_1(V)$ is the voltage measured at the pitot-tube1.

$$V_2 = \frac{-0.0001749 + \sqrt{(0.0001749)^2 + 4(0.00055)(Vol_{2i} - Vol_2)}}{2(-0.00055)} \quad (37)$$

where $Vol_{2i}(V)$ is the initial voltage measured at the pitot-tube2 when $V_2 = 0(\text{m/s})$, and $Vol_2(V)$ is the voltage measured at the pitot-tube2.

2.4 Replaceable Necks

As mentioned in the previous section, the resonance frequency of a Helmholtz resonator is dependent on the neck length, the cross-sectional surface area of the neck and the volume of the cavity. During the experiment, using pieces of duct with various lengths, we changed the flow velocity and the neck length to study the aeroacoustic source strength. Fig.(15) illustrates the model of a duct piece. These are the plastic duct pieces with approximately 3, 5, 6, 7, 14, 16, 20, 23 and 25 (cm) lengths named as replaceable neck length in the figures, and the other lengths are created by combinations of these with coupling clamps. Appendix B contains a table with explicit plastic duct lengths.

Calculating the total effective neck length, the following lengths are considered: the total of the neck length of two flasks, $0.095 \times 2(\text{m})$, (replaceable neck length) $\times 2$ (m), the total length of cross-junction and two coupling clamps, 0.196 (m) and the total length of the gaps like the one shown in Fig. (16), about 3.0×10^{-3} (m), which each clamp has.

³This way to compute the conversion equation is chosen because the fit of the data points in “Measured Voltage V.S. Anemometer Velocity” is better than the one in “Anemometer Velocity V.S. Measured Voltage”.

3 Results and Analysis

First of all, what is the APPROPRIATE strength to blow over the opening of the Helmholtz resonator to create a tone? The answer to this question will give us the first step to think about the aeroacoustic source strength, having insight to the timing when the energy dissipation happens. Then, looking into the relationship between the velocities before and after junction, we will have some ideas about the magnitude of the dissipated energy.

We will then examine the trends of the dissipated energy versus the Strouhal number. And also, the change in the quality factor lets us consider the energy efficiency inside our system.

3.1 Frequency Measurement

Analyzing this experiment with the assumption that the aeroacoustic system acts as a mass-spring system, the resonance frequencies are the first assumption to check. We started the theory for this experiment with the assumption of the resonance frequencies, $\frac{c}{2\pi} \sqrt{\frac{S_{neck}}{V_0 L'}}$. Fig. (17) illustrates the measured frequency versus Strouhal number. The frequencies measured with same neck lengths are about same for each neck lengths. Fig. (18) illustrates the measured frequency at each maximum of $\frac{Vac}{V_1}$ V.S. St for each neck length. Considering the uncertainty from the measurements of the flask volume, the cross-sectional surface area of the neck and the neck length, the measured frequency agrees enough with the theoretical model of Eq. (10). Therefore, our experiment is analyzable with this simple model.

3.2 Dimensionless Analysis: The Ratio $\frac{Vac}{V_1}$ V.S. Strouhal number

In order to know the range when the energy dissipation happens, a dimensionless quantity, $\frac{Vac}{V_1}$, is interesting to see compared with the corresponding Strouhal number, which is also a dimensionless quantity. However, it can be useful to analyze the pressure change in the resonators before considering the ratio, $\frac{Vac}{V_1}$. P_{amp} is the pressure amplitude in the flasks, and it is a quantity proportional to Vac as shown in Eq. (17). Fig. (19) shows $\frac{P_{amp}}{P_{atm}}$ V.S.

St using 0, 7, 16, 23, 25 and 30 (cm) straight replaceable necks where P_{atm} is atmospheric pressure. Since P_{atm} is a constant, it can be seen that, as St goes smaller, P_{amp} keeps increasing over our experimental range except for a quick drop at low St indicating a rapid shut-off of the sound ^{4 5}. So, V_{ac} can also increase like $\frac{P_{ac}}{P_{atm}}$ does. The ratio, $\frac{V_{ac}}{V_1}$, is interesting because it indicates the nature of the flow at the junction. From the ratio we can know the balance between acoustic flow at the junction and the main flow in the wind tunnel. This is important because the acoustic flow influences the shedding of vortices from the main flow which drive the acoustic resonance. Fig.(20) shows the $\frac{V_{ac}}{V_1}$ V.S. St using 0, 7, 16, 23, 25 and 30 (cm) straight replaceable necks, and Fig.(21) shows the results taken with longer necks: 25, 26, 27, 28, 29 and 30 (cm) straight replaceable necks, which are in the lower amplitude range ($\frac{V_{ac}}{V_1} \leq 0.1$). In region A, there is a moderate change in $\frac{V_{ac}}{V_1}$ V.S St . However in region B, there is a rapid change in $\frac{V_{ac}}{V_1}$ V.S St . Finally, we define region C to be $\frac{V_{ac}}{V_1} \leq 0.1$. The data shows the same general trend for all neck lengths. The acoustic amplitude increases with increased V_1 however, the ratio $\frac{V_{ac}}{V_1}$ reaches the point where increases in $\frac{V_{ac}}{V_1}$ become moderate. And then, moderately $\frac{V_{ac}}{V_1}$ reaches to the maximum value depending on V_1 characterized by each neck length. At sufficiently high V_1 , the resonance is extinguished as illustrated by the abrupt end of the data at low St . The ones with large $\frac{V_{ac}}{V_1}$ have the shear layer changing into vortices [4]. Additionally, longer necks and the right end of shorter necks generally have lower amplitude ($\frac{V_{ac}}{V_1} \leq 0.1$) indicating the importance of damping and the interaction between acoustic velocity and vortices [5]. Also, according to Elder and Howe, for the range, $\frac{V_{ac}}{V_1} \leq 0.1$, the oscillating pressure amplitude of the shear layer increases exponentially [6] [7]. In the range, $0.01 \leq \frac{V_{ac}}{V_1} \leq 0.1$, the acoustic field helps to form vortices [8].

⁴From Fig. (19), the maximum $\frac{P_{amp}}{P_{atm}}$ in our experimental range is 0.01284: multiplying by atmospheric pressure, the maximum P_{amp} is 1301 (Pa). From this result and the surface area of the flasks, the force exerting on the resonators' wall can be calculated as 194.9 (N). This oscillating force makes the glass vibrate at the highest amplitudes we measured. This vibrational energy should be included in any complete energy balance of the system.

⁵The maximum P_{amp} can also be written as the sound pressure level, 156,3 (dB). This is louder than the noise of military jet's taking off detected at 30(m) away from it.

3.3 Velocities Before and After the Opening of the Resonators

The kinetic energy difference before and after the cross junction allows us to compute $E_{dissipated}$. The relationship between V_2 and V_1 has allowed us to have insight into the trends of the $E_{dissipated}$ change.

Fig.(22) and (23) illustrates the relationship between V_2 and V_1 for the 0, 7, 16, 23, 25 and 30 (cm) straight replaceable necks. The grey line has slope 1. Until the point that resonance starts, $V_2 = V_1$, meaning that no work is done, and no energy is extracted from the flow. Once resonance starts, V_2 is slightly less than V_1 . Though not much, energy starts to be extracted. And then, there is decrease in V_2 for increase in V_1 indicating significant energy extracted from the mean flow going into acoustics. From the characteristic point illustrated as kinks in Fig. (22) and (23), the slope goes back to about 1 though the trend changes based on the neck lengths.

Looking at data taken with longer necks, which has low $\frac{Vac}{V_1}$, we can notice the small deviation from the line with slope 1 indicating we cannot use them to calculate the energy difference because of the low resolution of our pressure sensor and voltmeter. Considering Eq. (36) and (37) which are used to calculate the velocities before and after the junction, it is important to note the effect the difference between the initial voltage and the voltage measured when the air is flowing over the openings. As we can see from Fig. (13) and (14), more accurate voltage measurements are required for the low flow velocities than the higher ones. The Fluke 175 rms multimeter used as voltmeter for this experiment, can show four-digits; however, the smallest two-digits have had broad deviation.

3.4 Aeroacoustic Source Strength

$E_{dissipated}$ is the energy dissipated from the main stream in our setup. And $E_{acoustic}$ is the energy stored in acoustics instead of in vortices and other factors. Comparing these quantities, $E_{dissipated}$ and $E_{acoustic}$, we can get insight to the efficiency, which flow energy converts into acoustic energy.

3.4.1 Energy Dissipation

How efficiently is the flow energy dissipated at the junction? We can answer this question by taking the ratio of the kinetic energy of the flow measured before and after the junction. Fig. (24) shows the ratio versus St , and it illustrates an interesting result. Comparing with Fig. (20), when the change of $\frac{V_{ac}}{V_1}$ is rapid, the geometry (neck length) does matter to the percentage of the flow energy dissipated at the junction. However, once the change of $\frac{V_{ac}}{V_1}$ becomes moderate, we can see about 30 % of the flow energy dissipated at the junction for any geometry.

Fig. (25) shows $E_{dissipated}$ V.S. St using the results taken with 0, 7, 16 and 23(cm) replaceable necks. Because of the pressure sensor's low resolution, the (replaceable) neck length is limited to shorter than 25(cm). For ($\frac{V_{ac}}{V_1} \leq 0.1$), $E_{dissipation}$ increases rapidly. $E_{dissipation}$ continues to increase rapidly until a point corresponding to the $\frac{V_{ac}}{V_1}$ trend switching from rapid change to moderate one.

3.4.2 Quality Factor

As it is shown in the Theory section, the quality factor can be thought of as a ratio of the energy stored in acoustics to the total dissipated energy. So, the trend of the quality factor's change indicates the efficient conversion of flow energy into acoustic energy. By Fig. (24), we know about 30 % of the flow energy is dissipated at the junction. So, Q tells us the how much of the 30 % goes into acoustics. Fig. (26) illustrates Q V.S. St using the results taken with 0, 7, 16 and 23(cm) replaceable neck length. This trend also corresponds to $\frac{V_{ac}}{V_1}$. For the range, $\frac{V_{ac}}{V_1} \geq 0.1$, the similar increase and decrease as the graph of $\frac{V_{ac}}{V_1}$ is illustrated. For lower $\frac{V_{ac}}{V_1}$, we can see the trends, which are different trend from the ones with the higher $\frac{V_{ac}}{V_1}$.

3.4.3 Energy Balance

After examining Fig.(26), it is nice to see Fig. (27) which shows $E_{dissipated}$ and $E_{acoustics}$ using the result taken with 0(cm) replaceable neck length representing shorter neck's trend. At lower $\frac{Vac}{V_1}$, energy is dissipated for driving resonance inefficiently. The data points of the energy stored in acoustics do not overlap on the total energy dissipated in the junction. Instead of the energy stored in acoustics, there are other factors that dominate the energy converted from the flow energy. Around the maximum $\frac{Vac}{V_1}$, less energy is dissipated from the main flow for driving resonance. Since the energy stored in acoustics is just a part of the total dissipated energy, usually $E_{acoustics}$ is lower than $E_{dissipated}$. However, around the maximum $\frac{Vac}{V_1}$, we can see higher $E_{acoustics}$ than $E_{dissipated}$.

4 Conclusion

In order to determine the characteristic of the aero-acoustic excitation of Helmholtz resonators with different neck geometries and the work done to sustain and excite resonance, we have used a system with two Helmholtz resonators positioned at opposite sides of a junction in a wind tunnel. The air flowing over the junction openings to the Helmholtz resonators can excite the acoustic resonance of the system. The work done by the aero-acoustic source of sound has been determined through the measurement of the air speed in front of and behind the junction in the wind tunnel; and, the energy stored in the resonator has been determined through the measurement of the acoustic pressure inside the resonator's cavity. We intend to redo this experiment with an improved method to get more accurate flow velocities inside the duct before and after the junction. As it is mentioned in the section titled "Velocities Before and After the Opening of the Resonators", we need to increase the resolution of the velocity measurement for the low speeds. Physically, the pitot-tubes detect not only the air flow straight into the surface of the hole, but also the rotating turbulent flows (See Fig. (28)). In order to avoid this, hot wire anemometry can be used instead of pitot-tubes. By the improved measurement, the quality factors in the low amplitudes' range can be determined [9].

Additionally, getting more insight to what happens inside the wind tunnel and resonators, it could be interesting to see the form of flow using a smoke machine.

5 Acknowledgements

I am grateful to my research advisor, Dr. William V. Slaton, for supporting and giving me an opportunity to have pleasant time working on the research.

I would like to thank the department of Physics and Astronomy for support.

I am also thankful to the Acoustic Society of America for the Robert Young Award and CNSM Student Research Fund which I received for this work.

6 Reference

- [1] Lawrence E. Kinsler, Austin R. Frey, Alan B. Coppens, and James V. Sanders. *Fundamentals of Acoustics*, 4th edition. John Wiley & Sons, Hoboken, NJ
- [2] R. Byron Bird, Warren E. Stewart, and Edwin N. Lightfoot. *Transport Phenomena*. John Wiley & Sons, New York, NY, 1960.
- [3] P. A. Aswatha Narayana, and K. N. Seetharamu. *Engineering Fluid Mechanics*. Alpha Science International Ltd., Harrow, U.K., 2005.
- [4] P. A. Nelson, N.A. Halliwell, and P. E. Doak. *Fluid Dynamics of a Flow Excited Resonance*. Part II: Flow Acoustic Interaction. *J. Sound. Vib.*,91:375-402, 1983.
- [5] Peters, Marinus Carolus Adrianus Maria. *Aeroacoustic Source In Internal Flows.*, 1988.
- [6] S. A. Elder. *Forced Oscillations of a Separated Shear Layer with Application to Cavity Flow-Tone Effects*. *J.Acoust. Japan*, 67:774-781, 1980.
- [7] M. S. Howe. *Acoustics of Fluid-Structure Interactions*. Cambridge University Press, 1998.
- [8] S. Ziada and E. T. Buhlman. *Self-Excited Resonances of Two Side Branches in Close Proximity*. *J. Fluids. Struct.*, 6:583-601, 1992.
- [9] A. D. Pierce. *Acoustics: An Introduction to Its Physical Principles and Applications*. Acoustical society of America Edition, 1989.

7 Appendix

A The Derivation of the Ratio, $\frac{\langle V \rangle}{V_{max}}$, for Turbulent Flow

Experimentally, turbulent velocity V_z and the maximum velocity $V_{z,max}$ are given roughly by

$$\frac{V_z}{V_{z,max}} = \left(1 - \frac{r}{R}\right)^{1/7} \quad (38)$$

where r and R are defined in Fig. (29) [2]. And the turbulent and a laminar flows distributions are illustrated in Fig. (30) [2]. Solving Eq. (38) for V_z ,

$$V_z = V_{z,max} \left(1 - \frac{r}{R}\right)^{1/7}. \quad (39)$$

Then, the area average velocity is,

$$\begin{aligned} \langle V_z \rangle &= \frac{1}{S} \int_S V_{z,max} \left(1 - \frac{r}{R}\right)^{1/7} dS \\ &= \frac{2\pi}{\pi R^2} \int_0^R V_{z,max} \left(1 - \frac{r}{R}\right)^{1/7} r dr \end{aligned} \quad (40)$$

Letting $u = \left(1 - \frac{r}{R}\right)$,

$$\begin{aligned} \langle V_z \rangle &= \frac{2\pi V_{z,max}}{\pi R^2} \int_1^0 u^{1/7} (u-1) R^2 du \\ &= 2V_{z,max} \int_1^0 u^{8/7} - u^{1/7} du \\ &= 2V_{z,max} \left\{ -\frac{7}{15} + \frac{7}{8} \right\} \\ &= \frac{49}{60} V_{z,max} \\ &\simeq 0.80 V_{z,max}. \end{aligned} \quad (41)$$

B The Measured Length of the Replaceable Duct Pieces.

Ideal Length (cm)	Measured Length (cm)
3	3.00 ± 0.005
5	5.00 ± 0.005
6	5.95 ± 0.005
7	6.95 ± 0.005
14	13.85 ± 0.005
16	16.00 ± 0.005
20	19.80 ± 0.005
23	22.95 ± 0.005
25	24.70 ± 0.005
30	30.02 ± 0.005

C Figures

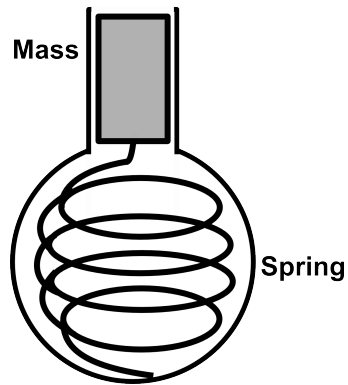


Figure 1: Mass-spring system in an empty bottle

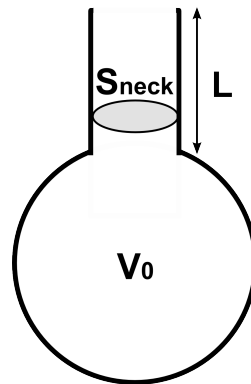


Figure 2: Helmholtz resonator

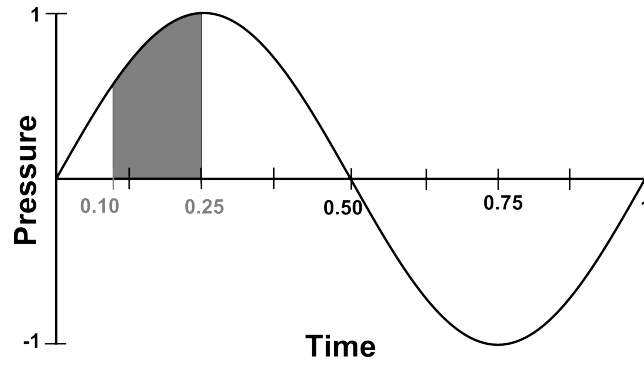


Figure 3: The change of the pressure inside the flask V.S. time in a period.

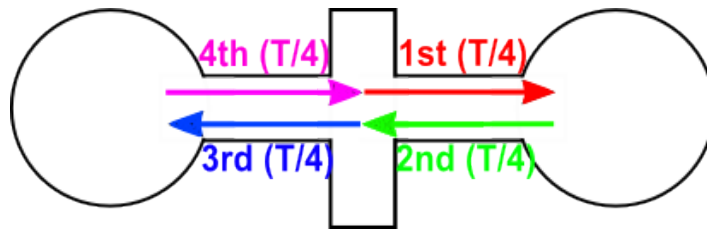


Figure 4: The movement of the air in the neck during a period.

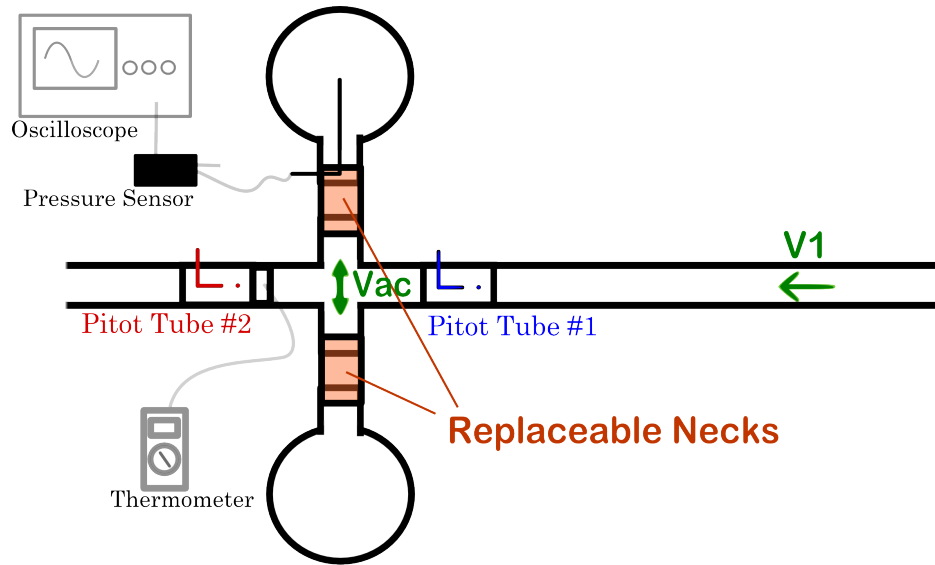


Figure 5: Whole system

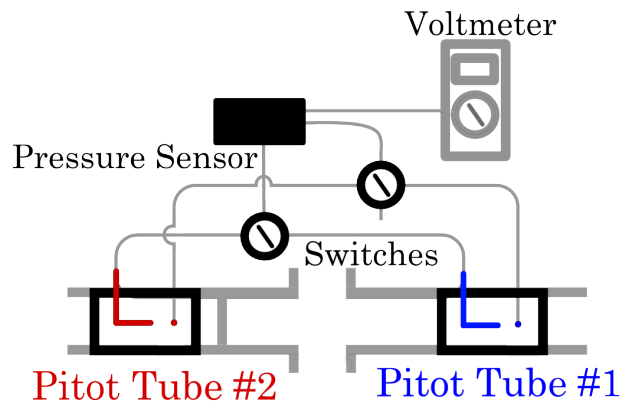


Figure 6: The system around the pitot-tube measuring the velocities in the main wind tunnel

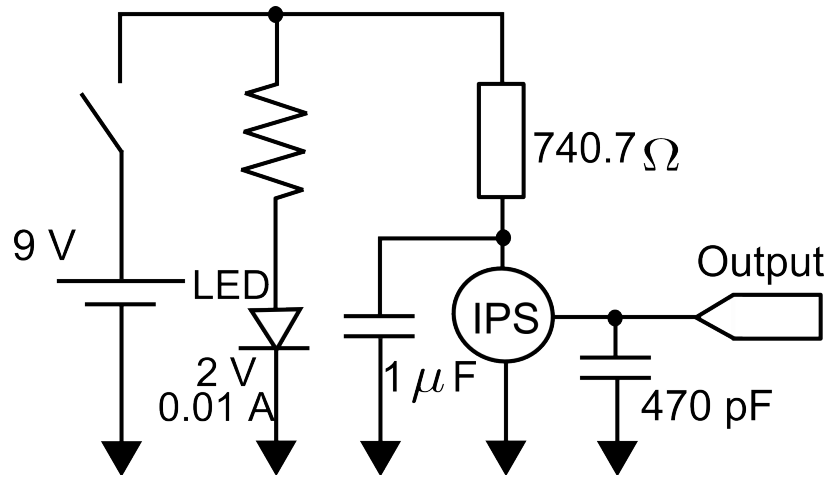


Figure 7: The circuit diagram of the pressure sensor black boxes

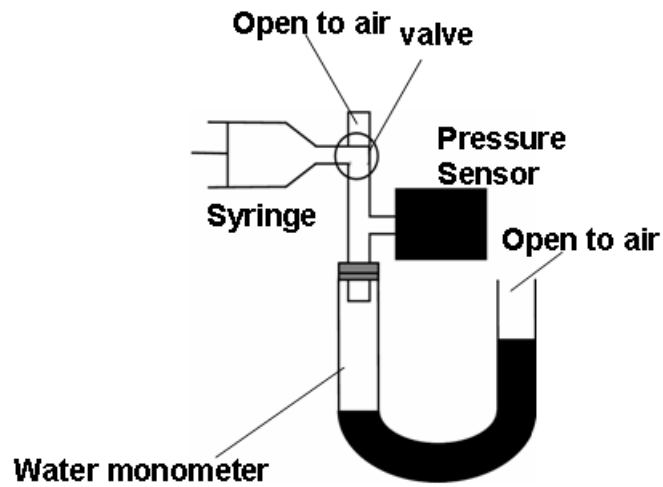


Figure 8: The system for the calibration of the pressure sensor for P_{amp} measurement

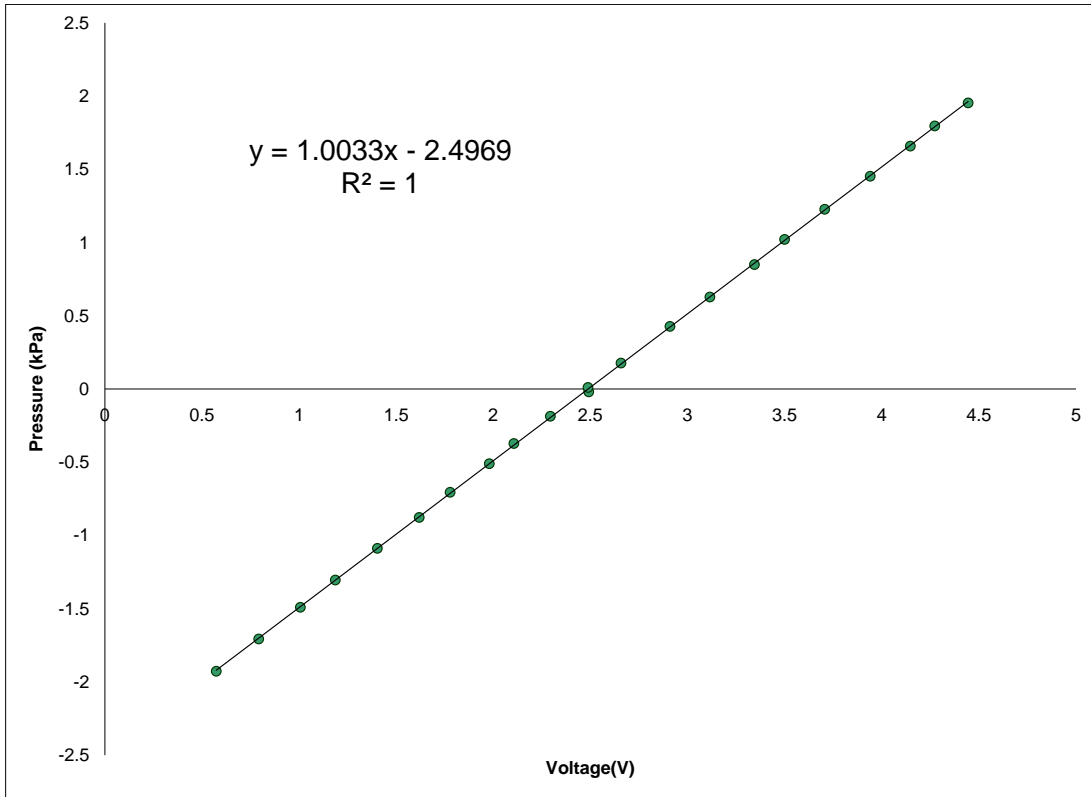


Figure 9: The calibration graph of the pressure sensor measuring the pressure inside the flask

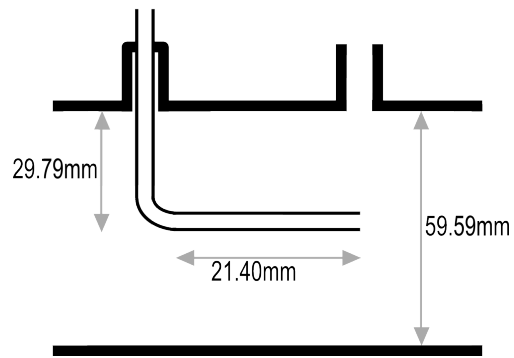


Figure 10: The model of a pitot-tube

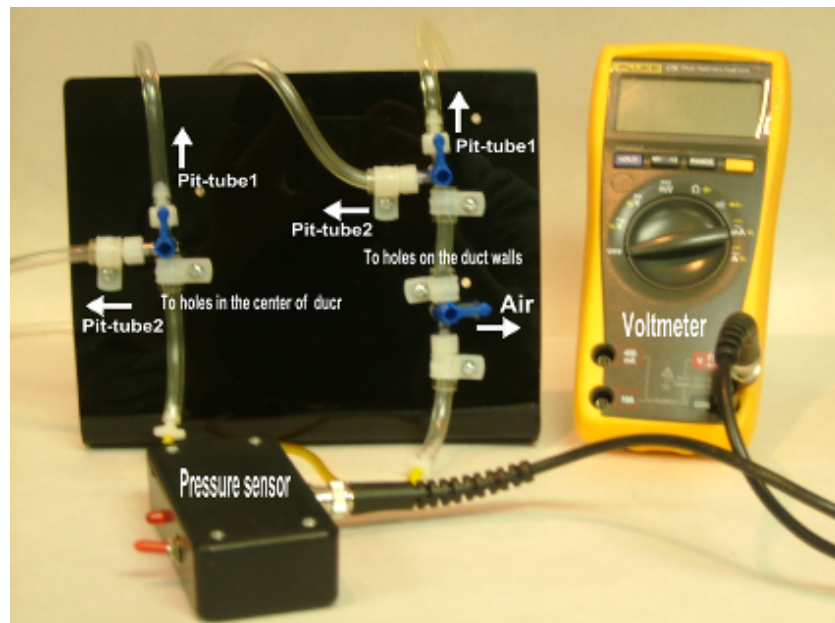


Figure 11: The picture of the switches connected to the pressure sensor and the voltmeter

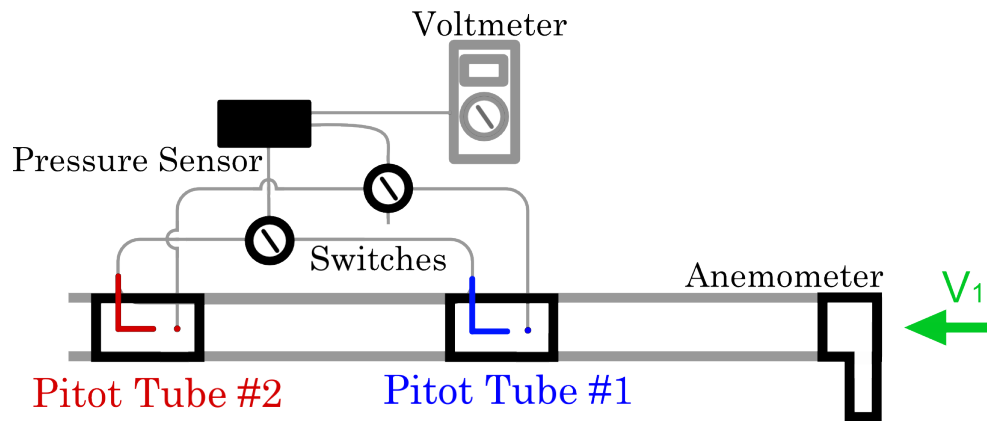


Figure 12: The Set up for pitot-tube calibration

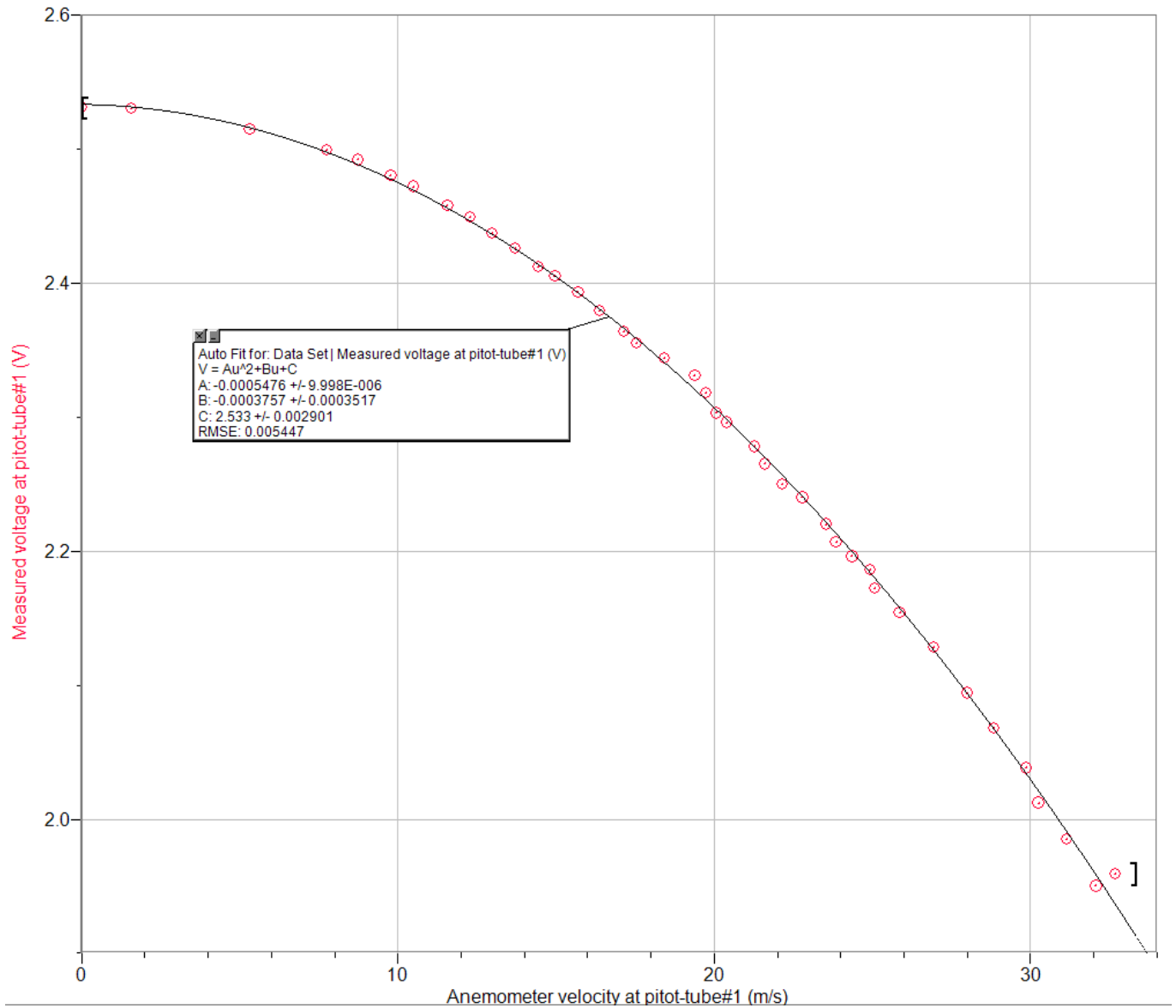


Figure 13: The calibration graph for pitot-tube1

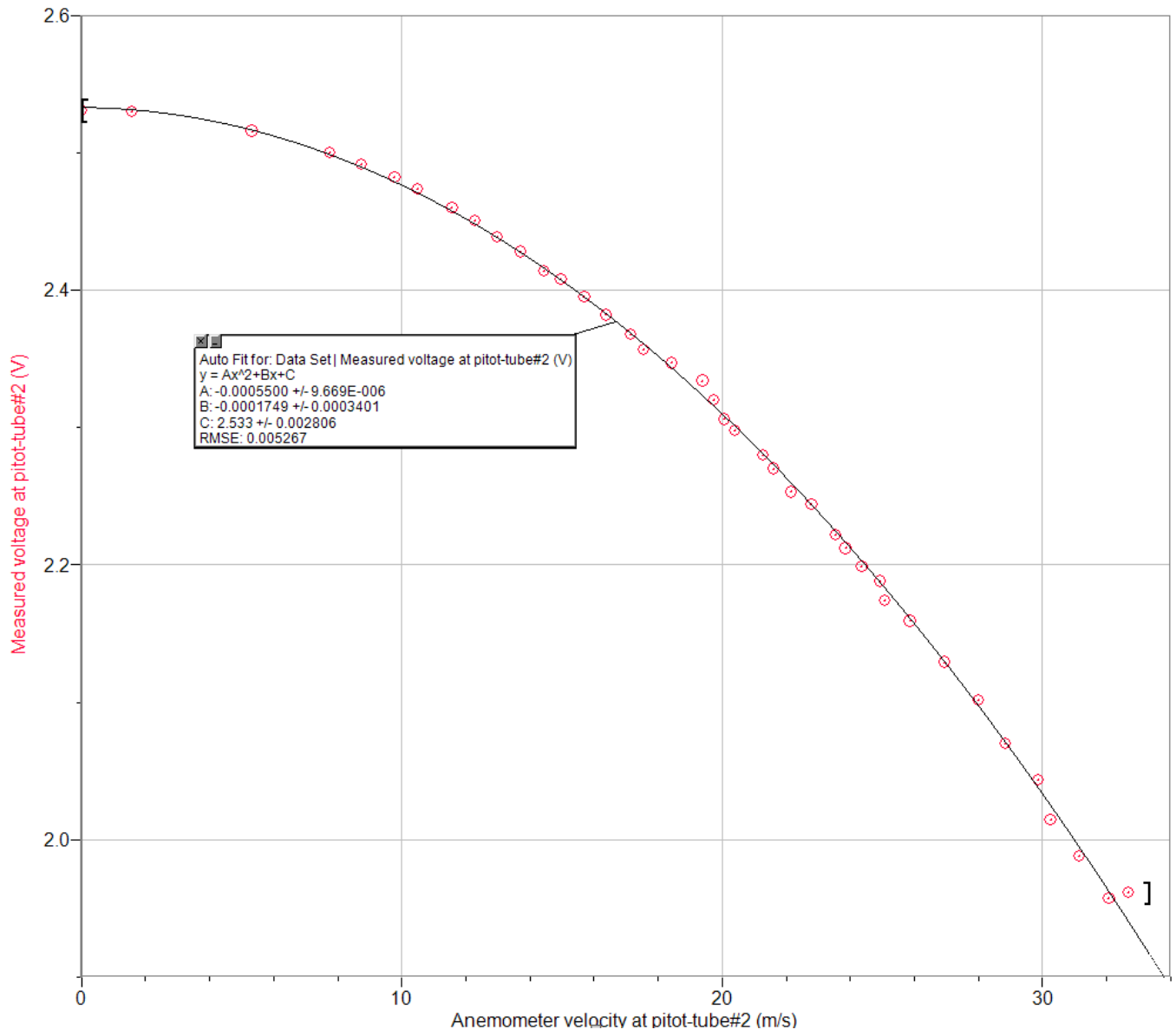


Figure 14: The calibration graph for pitot-tube2

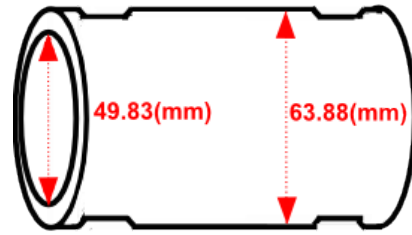


Figure 15: The model of duct piece for replacing the neck length of Helmholtz resonators.



Figure 16: A coupling clamp.

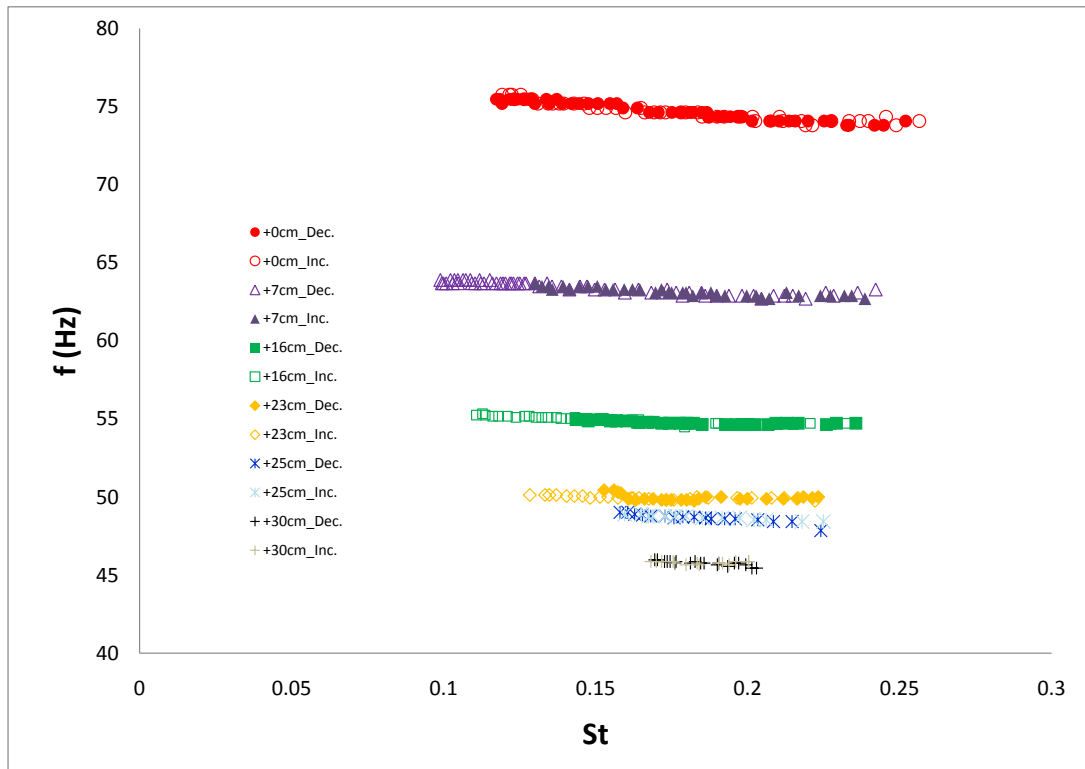


Figure 17: f V.S. St using the data taken with 0, 7, 16, 23, 25 and 30 (cm) replaceable necks. “Inc.” = the data taken when the flow is increasing. “Dec.” = the data taken when the flow is decreasing.

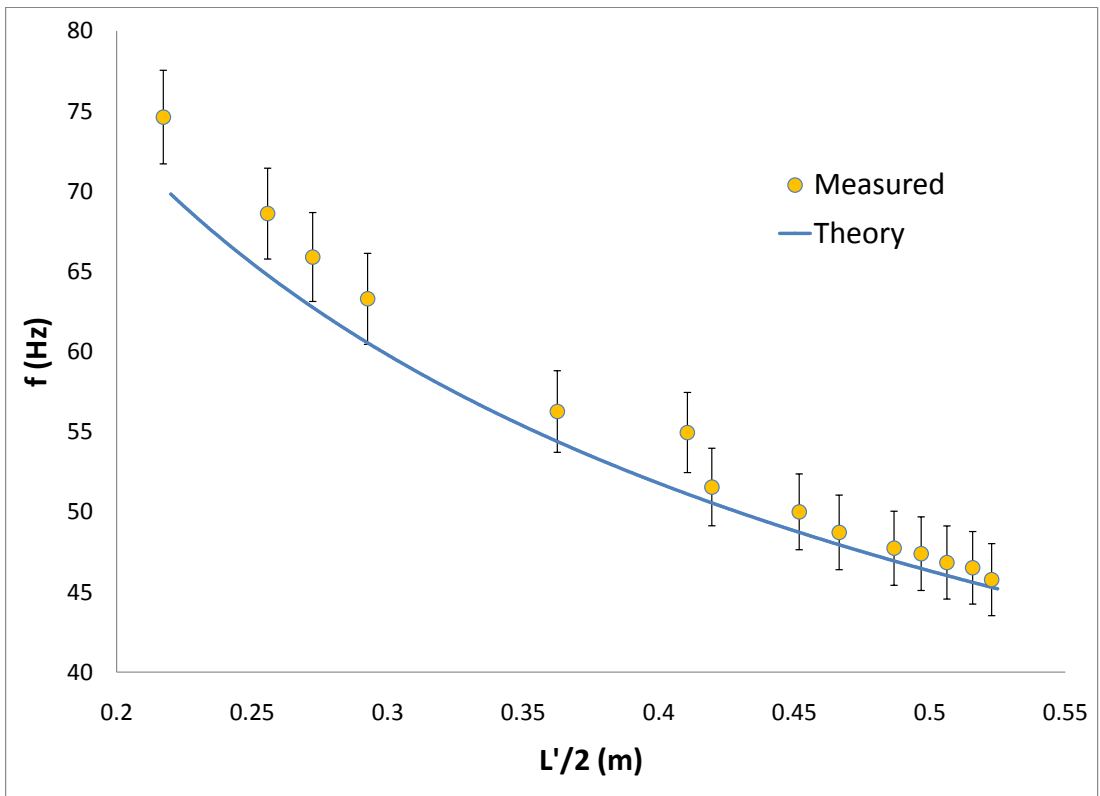


Figure 18: f at the each maximum $\frac{V_{ac}}{V_1}$ for each replaceable neck length

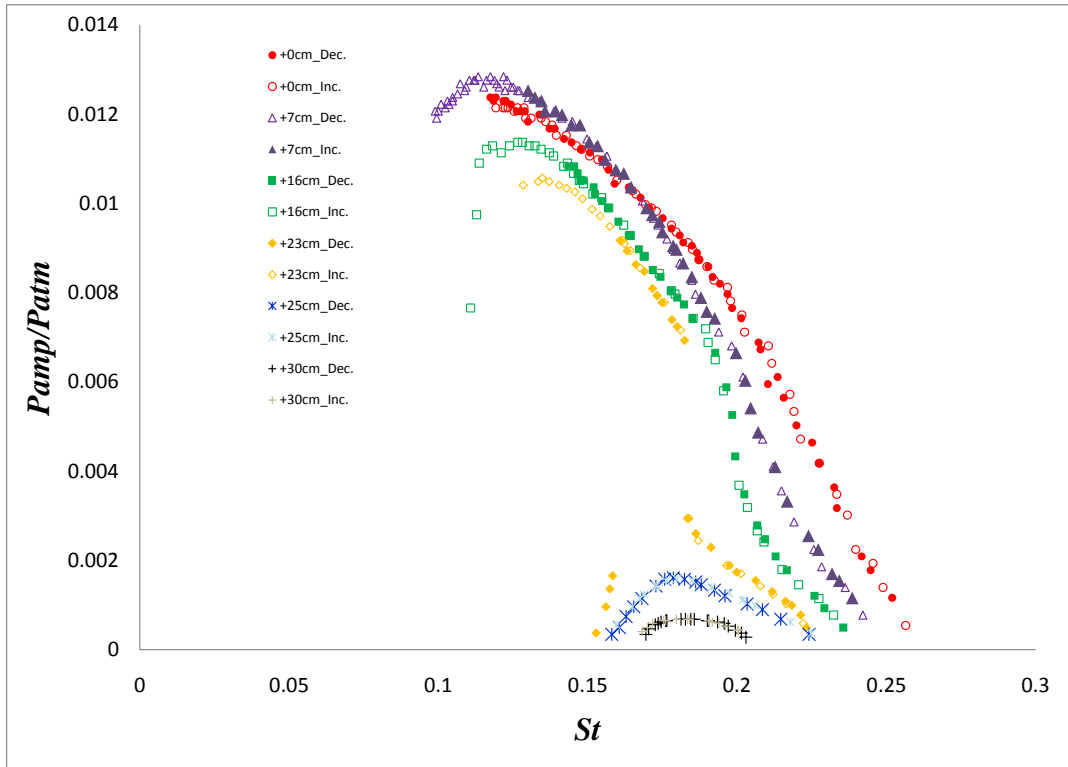


Figure 19: $\frac{P_{amp}}{P_{atm}}$ V.S. St using the data taken with 0, 7, 16, 23, 25 and 30 (cm) replaceable necks. “Inc.” = the data taken when the flow is increasing. “Dec.” = the data taken when the flow is decreasing.

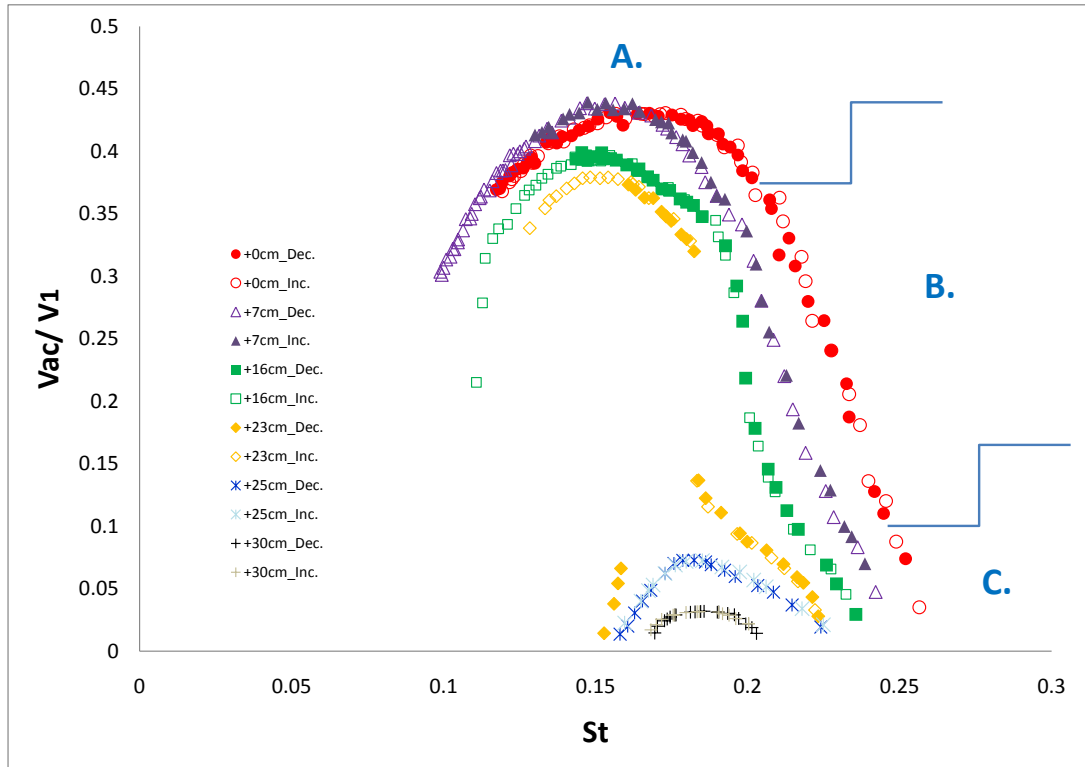


Figure 20: $\frac{V_{ac}}{V_1}$ V.S. St using the data taken with 0, 7, 16, 23, 25 and 30 (cm) replaceable necks. “Inc.” = the data taken when the flow is increasing. “Dec.” = the data taken when the flow is decreasing. Region A : the range with moderate change in $\frac{V_{ac}}{V_1}$, region B : the range with rapid change in $\frac{V_{ac}}{V_1}$, and region C : $\frac{V_{ac}}{V_1} \leq 0.1$.

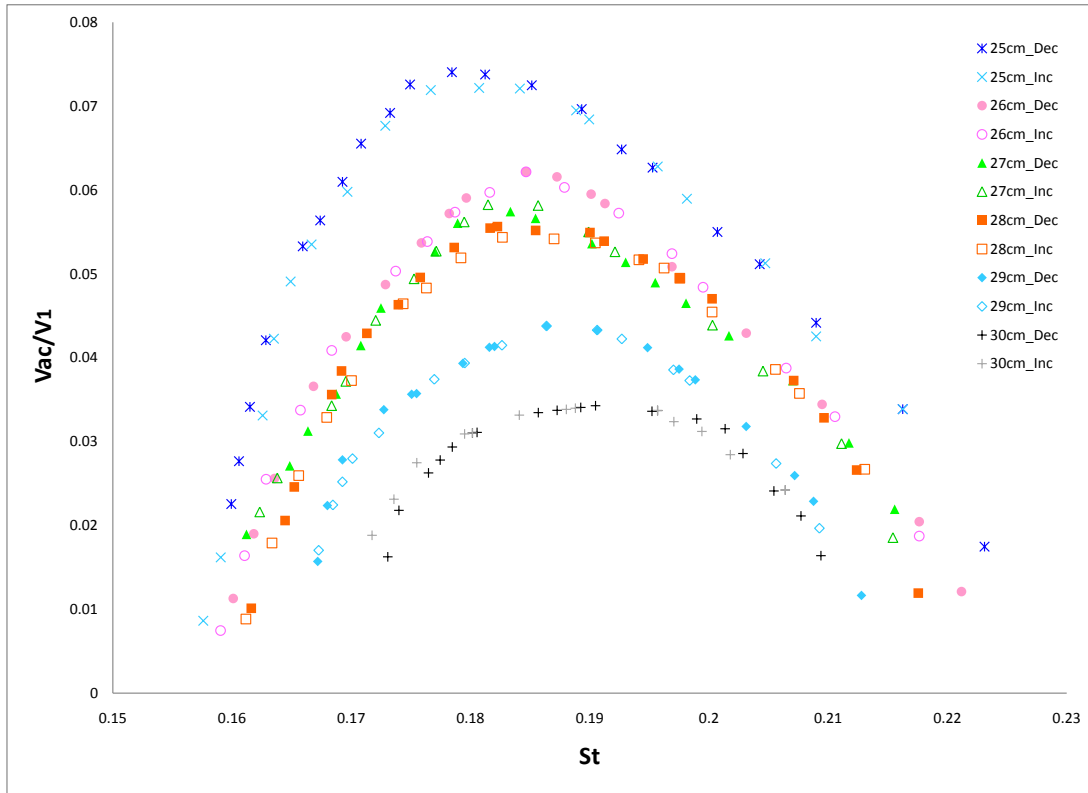


Figure 21: $\frac{V_{ac}}{V_1}$ V.S. St using the data taken with longer necks, 25, 26, 27, 28, 29 and 30 (cm) replaceable necks. “Inc.” = the data taken when the flow is increasing. “Dec.”= the data taken when the flow is decreasing.

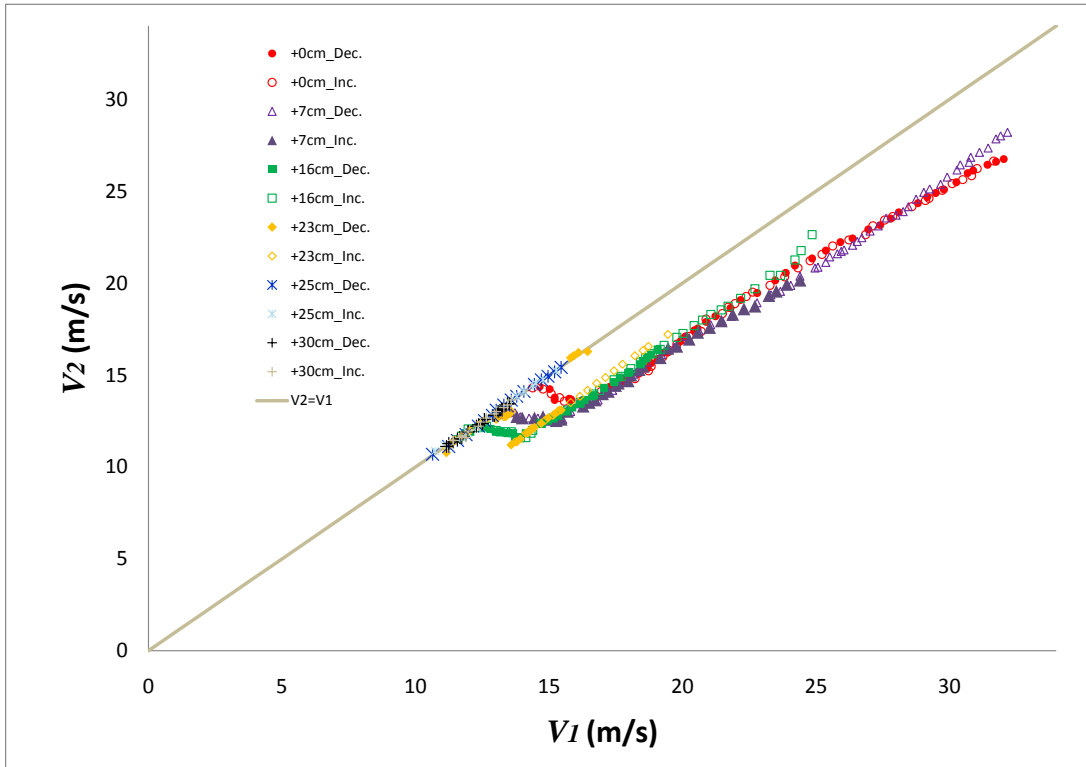


Figure 22: The relationship between V_2 and V_1 of the data-sets taken with the 0, 7, 16, 23, 25 and 30 (cm) replaceable necks. “Inc.” = the data taken when the flow is increasing. “Dec.” = the data taken when the flow is decreasing.

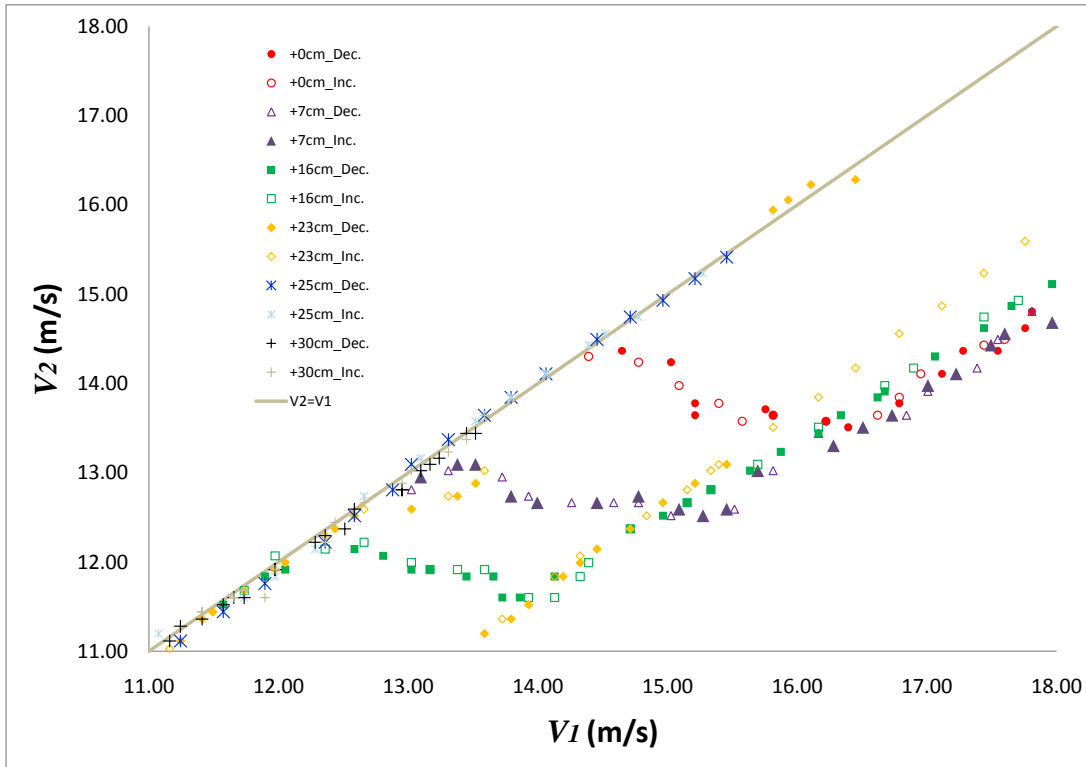


Figure 23: The relationship between V_2 and V_1 of the data-sets taken with the 0, 7, 16, 23, 25 and 30 (cm) replaceable necks focused on a particular range $11 \leq V_1 \leq 18$ (m/s). “Inc.” = the data taken when the flow is increasing. “Dec.” = the data taken when the flow is decreasing.

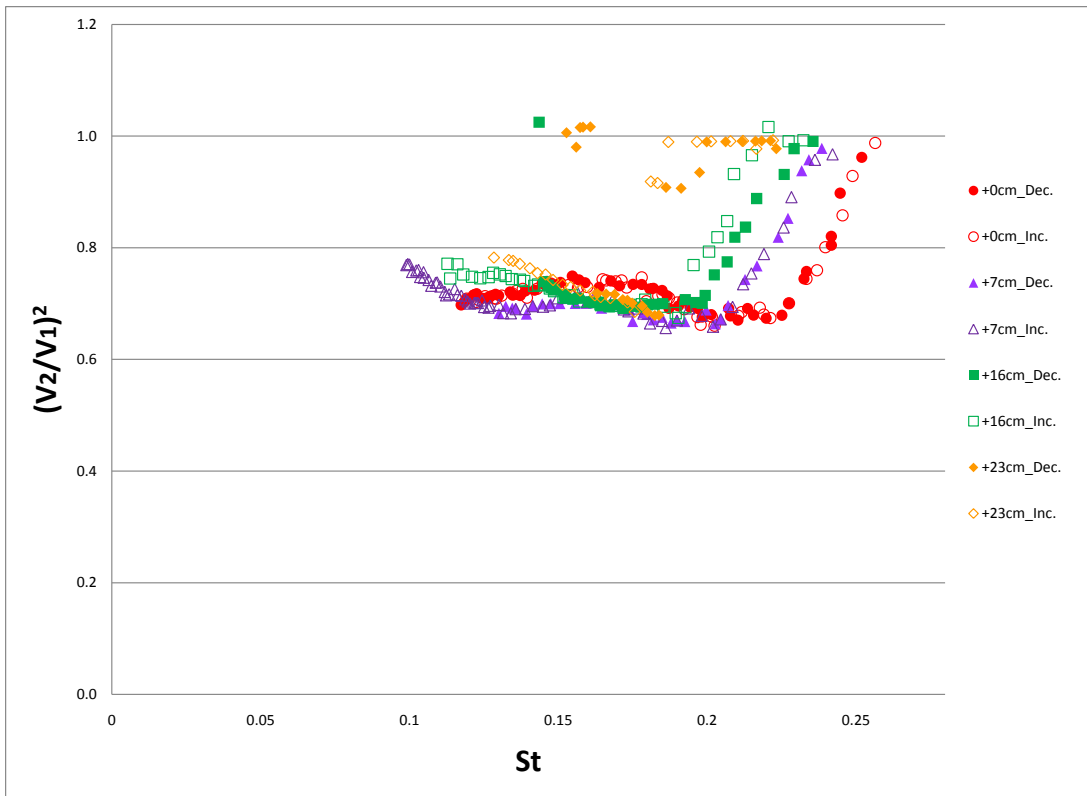


Figure 24: The ratio of the energy measured after the junction to the one before the junction $V.S.$ St using data-sets taken with 0, 7, 16 and 23 (cm) replaceable necks. “Inc.” = the data taken when the flow is increasing. “Dec.” = the data taken when the flow is decreasing.

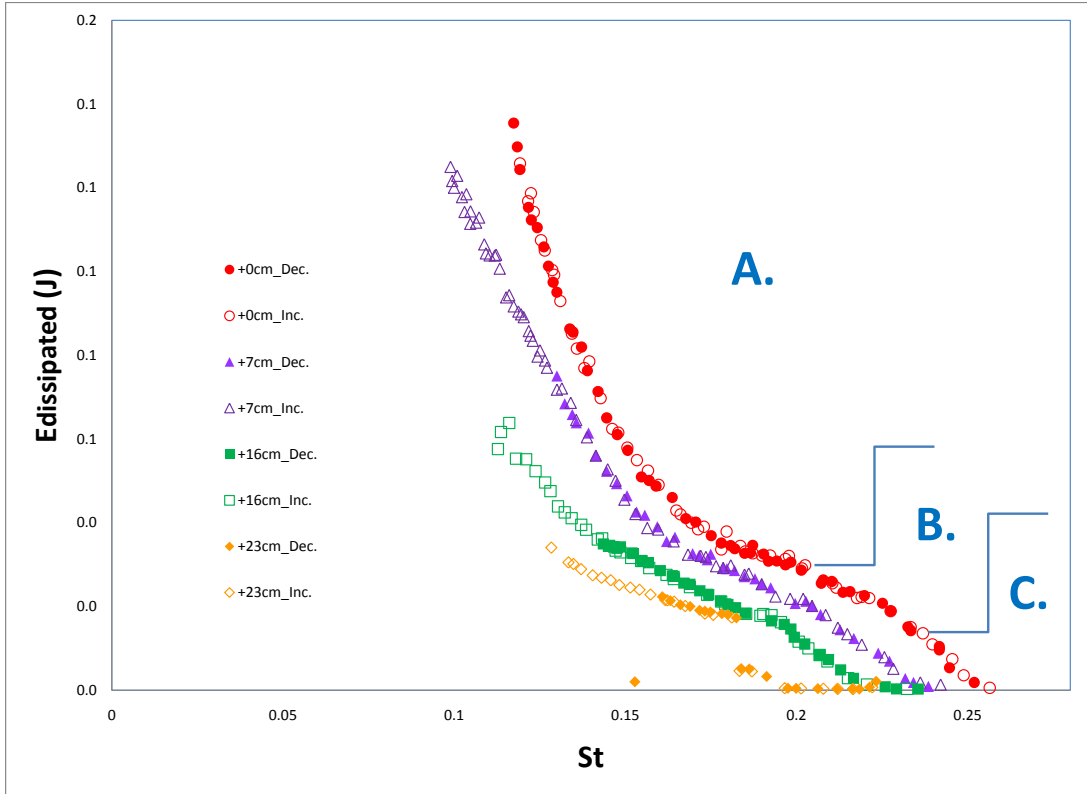


Figure 25: The measured dissipated energy V.S. St using data-sets taken with 0, 7, 16 and 23 (cm) replaceable necks. “Inc.” = the data taken when the flow is increasing. “Dec.” = the data taken when the flow is decreasing. Region A : the range with moderate change in $\frac{V_{ac}}{V_1}$, region B : the range with rapid change in $\frac{V_{ac}}{V_1}$, and region C : $\frac{V_{ac}}{V_1} \leq 0.1$.

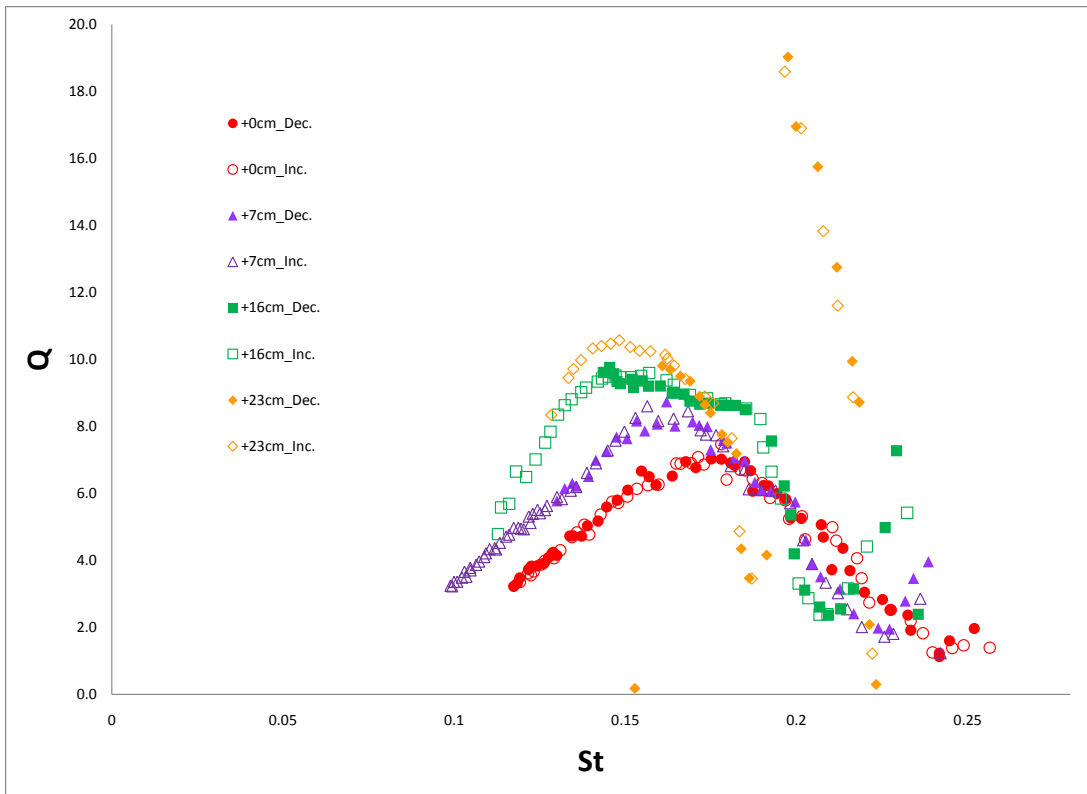


Figure 26: Quality factor V.S. St using data-sets taken with 0, 7, 16 and 23 (cm) replaceable necks. “Inc.” = the data taken when the flow is increasing. “Dec.” = the data taken when the flow is decreasing.

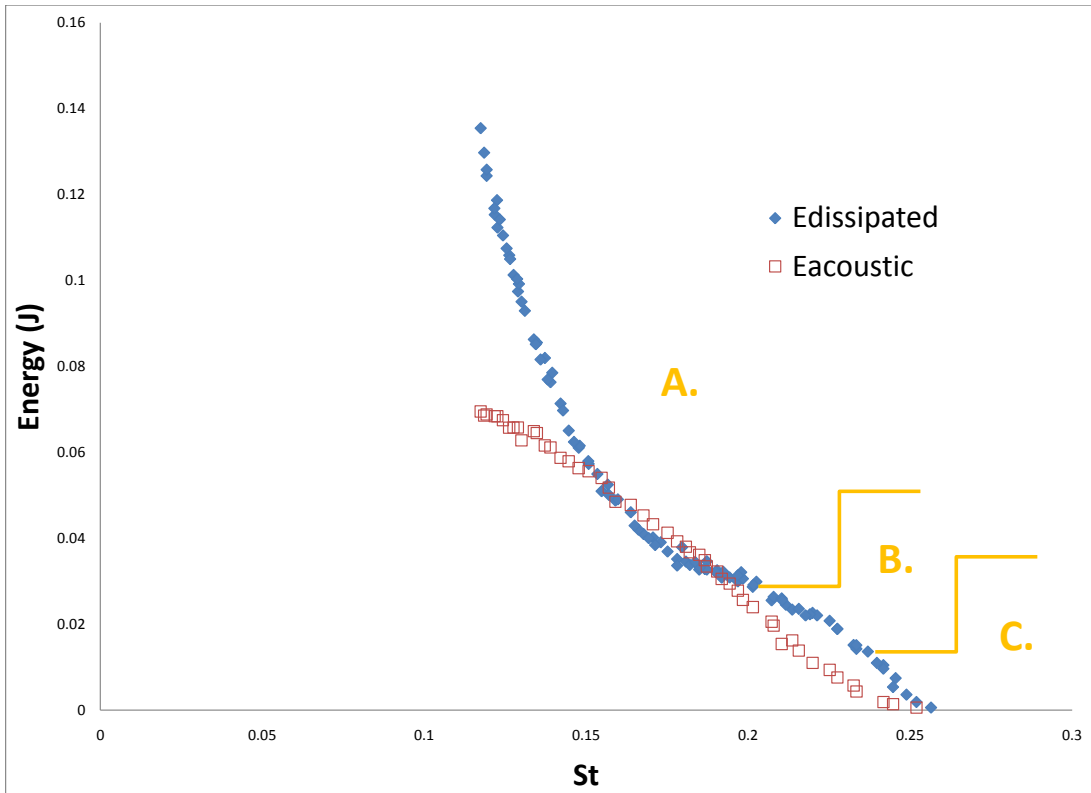


Figure 27: $E_{dissipated}$ V.S. $E_{acoustics}$ using the data-set taken with 0(cm) replaceable neck. Region A : the range with moderate change in $\frac{V_{ac}}{V_1}$, region B : the range with rapid change in $\frac{V_{ac}}{V_1}$, and region C : $\frac{V_{ac}}{V_1} \leq 0.1$.

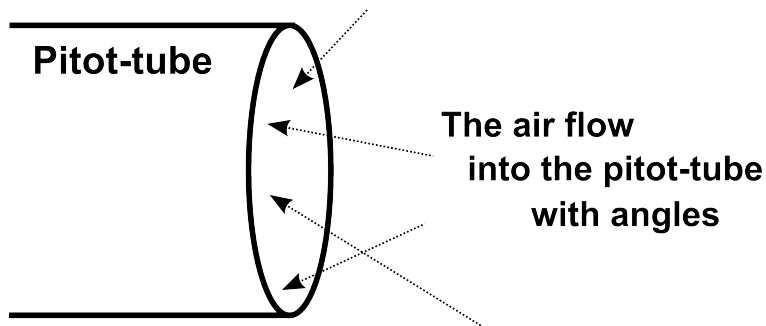


Figure 28: Expected air flow into a pitot-tube

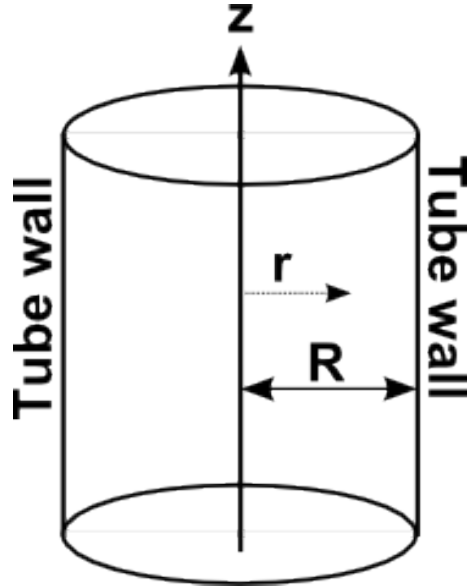


Figure 29: The supplemental picture.

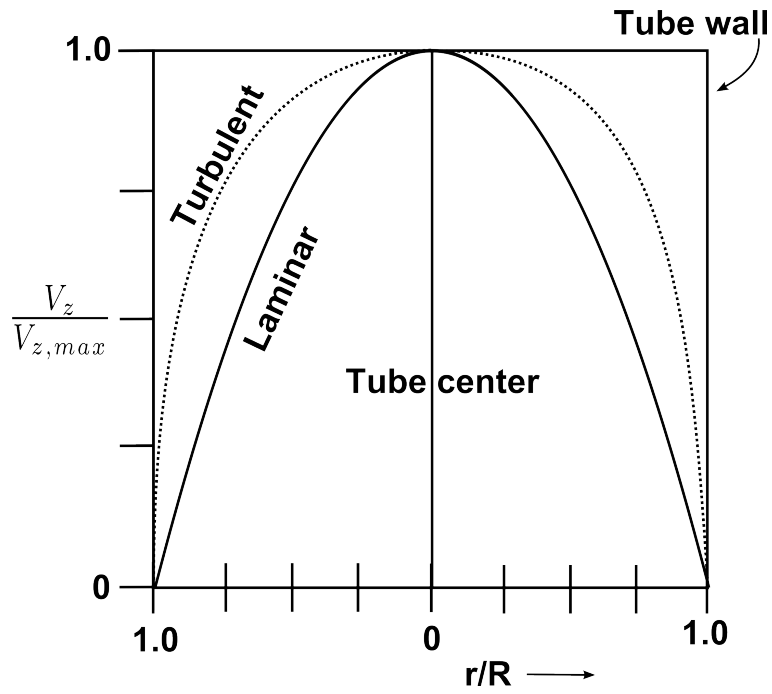


Figure 30: Laminar and turbulent velocity distributions.